PAT

Monitoring the relaxation behavior of nylon/clay nanocomposites in the melt with an online dielectric sensor[†,‡]

Yu-Hsin Lee, Anthony J. Bur*, Steven C. Roth, Paul R. Start and Richard H. Harris

National Institute of Standards and Technology, Gaithersburg, MD 20899, USA

Dielectric spectrometry was used to correlate microstructure of the filler with relaxation behavior of the polymer matrix in nylon/clay nanocomposites. Agglomerated, intercalated, and exfoliated composites were fabricated by extruding nylon 6 and nylon 12 with montmorillonite clays treated by two types of amino surfactants. A new on-line dielectric slit die sensor was used to examine the melt state properties during extrusion compounding in a frequency range from 50 to 10^6 Hz. Using non-linear regression methods, the experimental data were fit with the Cole–Cole dielectric relaxation functions corrected for electrode polarization and d.c. conductivity. Characteristic frequency, relaxation strength, relaxation time distribution, as well as d.c. conductivities were extracted from curves with overlapping relaxation modes. Only one dielectric dispersion was found in the neat nylon, which was identified as α relaxation associated with molecular segmental motion. Two dielectric relaxations, α relaxation and Maxwell–Wagner–Sillars interfacial polarization (MWS), were observed in the composite melt. MWS is ascribed to conducting ions in a polymer/filler mixture and has relaxation properties that are dependent upon the microstructure of the filler. Published in 2005 by John Wiley & Sons, Ltd.

KEYWORDS: clay; dielectric properties; microstructure; nanocomposites; polyamides

INTRODUCTION

Polymer/clay nanocomposite research during the past decade has focused on the formulation and compounding of different polymer/clay combinations in conjunction with the impact of morphology on material properties such as modulus, yield strength, and fire retardation in the solid state.[1–4] Fewer efforts have been made on the investigation of relaxation behavior of the resin,[5,6] especially in the melt state. In this article, the application of a new dielectric slit die sensor used to monitor dielectric properties of nylon/clay nanocomposites during extrusion from a twin-screw extruder is reported on. The on-line dielectric sensor provides insights on how the polymer dynamics on the molecular level are altered with regard to the matrix type, the filler loading, and the morphology of the nanocomposites. Dielectric data enables one to distinguish the relative degree of clay exfoliation between samples but the microstructure of the clay cannot be identified by using dielectric spectrometer alone. Consequently, data obtained from the on-line dielectric instrument are correlated with off-line transmission emission microscopy (TEM) and X-ray diffraction (XRD) to establish the relationship between the filler dispersion and dielectric relaxation behavior of polymer resin in the molten state.

Dielectric relaxation spectroscopy (DRS) is a powerful technique for obtaining dipolar relaxation as a function of temperature and frequency from which effects due to intermolecular cooperative motion and hindered dipolar rotation can be elucidated. Dielectric relaxations arise when polar segments of the polymer chains orient under the influence of an alternating electric field. For α relaxation, which is associated with the glass transition, it is a process in which a number of amorphous chains relax simultaneously in a cooperative motion. In addition to the α relaxation, a Maxwell–Wagner–Sillars interfacial polarization (MWS)[7–10] may be observed in any heterogeneous systems due to the accumulation of charge at the interface of two media having different permittivities and/or conductivities. The characteristic frequency of MWS reflects the time scale of rearrangements of the charges, which piled up at the interface. The MWS formulae for various heterogeneous systems depend strongly upon the geometry of the interface or the shape of the dispersed particles.[7–10] The relaxation time distribution was used as a rough indicator to describe the heterogeneity of the polymer/filler interface. MWS can be distinguished from the α relaxation by its larger dielectric intensity.

This program was initiated with the hypothesis that filler dispersed throughout the polymer matrix will modify

Correspondence to: A. J. Bur, 100 Bureau Drive, Mail stop 8542, Gaithersburg, MD 20899-8542, USA.
E-mail: anthony.bur@nist.gov

dielectric relaxation behavior in a manner that reflects the morphology of the composites. Therefore, the relaxation parameters that emerge from on-line dielectric data serve as excellent indicators to differentiate exfoliation from intercalation or agglomeration.

EXPERIMENTAL[a]

Sample preparation

Nylon 6 (Capron 8200NL) obtained from Honeywell[a] and nylon 12 (Grilamide L16 natural) obtained from EMS Chemie are medium viscosity resins with nominal melting temperatures (T_m) of 225 and 195°C, respectively. Two organically modified clays, obtained from Southern Clay products,[a] Cloisite 15A (15A) and Cloisite 30B (30B), were used as received and compounded at a 2 and 4% mass fraction of clay in nylon 6 and at a 4% mass fraction of clay in nylon 12. 15A is prepared by ion exchange of naturally occurring sodium with a quaternary ammonium ion (dimethyl, dihydrogenatedtallow, quaternary ammonium). Similarly, 30B is ion exchanged for a methyl, tallow, bis-2-hydroxyethyl, quaternary ammonium ion. The two clays differ not only by the surfactant functionality, which is polar for 30B and non-polar for 15A but also the surfactant content, which is 1.35 cation exchange capacity (CEC) for 15A and 0.97 CEC for 30B.

Prior to extrusion compounding, both resin pellets and the clay powders were dried in vacuum for 12 hr at 80°C. To prepare 2 and 4% mass fraction of clay in the resin, 200 g batches of dry nylon pellets and silicate powders were hand mixed in a beaker and transferred to a twin-screw extruder feeder. An 18 mm Haake Rheocord model 9000 twin-screw extruder operating at 30 rpm was used. The residence time for compounding in the extruder was approximately 4 min. The processing temperature for nylon 6 and its composites is 240°C and 195°C for nylon 12 and its composites.

Instrumentation

The on-line dielectric measurement sensor was recently developed to study dielectric properties of polymer composites in the melt phase.[11,12] Figure 1 is a side view of the dielectric cell showing the flow-through slit, the interdigitating electrodes, and the standard 12.7 mm instrument ports. The cell has a stainless steel housing consisting of top and bottom halves. An alumina ceramic block with interdigitating platinum electrodes, that have been fired into the ceramic, is placed into the bottom half of the stainless steel housing. A temperature-controlled heating jacket is clamped around the unit. In operation, the dielectric cell is fastened onto the end of the extruder monitoring the resin during flow through the slit. When a voltage (1 V_{rms}) is applied to the interdigitat-
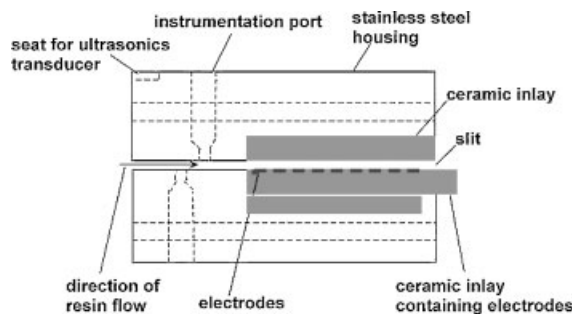
Figure 1. Side view of the dielectric slit die. The size of the slit is 2 mm and the length of die is 180 mm.

ing electrodes, an electric field extends into the molten resin flowing through the slit channel. By measuring the in-phase and out-of-phase components of the current flowing through the resin, the complex relative permittivity, $\varepsilon^* = \varepsilon' - i\varepsilon''$, is measured. The relative standard uncertainty in the measured ε' and ε'' data is 1% and the standard uncertainty of the temperature, which is regulated by the on-line heating jacket, is 1°C.

The dielectric cell is connected to a computer-controlled lock-in amplifier, (Stanford Research model SR810), which, in conjunction with instrument software, operates as a dielectric spectrometer (the CEP Proceptor) and yields relative permittivity at 14 discrete frequencies in the range 50 to 10^5 Hz. More details regarding the interdigitating electrode measuring technique and the dielectric slit die design can be found elsewhere.[13–15]

Morphological characterization of the composites was carried out by XRD and TEM. XRD samples were prepared by molding the material at the same temperature used for processing (240°C for nylon 6 and 195°C for nylon 12) into plaques which are 20 mm by 20 mm square with a thickness of 2 mm. XRD data were collected by using a Philips Electronic Instruments XRG 3100 X-ray Generator with an automatic sampler. X-ray beam was produced by copper K alpha radiation at 1.54 A. XRD measurements were made every 0.04° between 2° and 12°. TEM specimens were cut from extruded samples using a Leica cryo-ultramicrotome, equipped with a diamond knife. Sectioning was performed at −80°C. Sections were collected from the knife edge and placed onto 400 mesh copper-rhodium grids. TEM micrographs were taken with a Philips EM400C at an accelerating voltage of 120 kV.

Data analysis

The dielectric properties of molten polymers contain conducting ions that contribute to both d.c. conductivity and electrode polarization effects.[16] The large increases at low frequencies in both the ε' and ε'', observed in most polymers at high temperature, are evidences of these two effects and must be corrected for in order to quantify the material dielectric properties. This is accomplished by modeling the electrode as a capacitance/resistance parallel circuit that is in series with the sample, and d.c. conductivity as a resistance in parallel with the sample.[12,16] The situation can be described as an electrode admittance Y_{el} in series with the sample

PAT

admittance Y_s. These admittances add to yield the apparent admittance Y_{app},

$$Y_{app} = G_{app} + i\omega C_{app} = \frac{Y_{el}Y_s}{Y_{el} + Y_s} \qquad (1)$$

where G_{app} and C_{app} are the apparent conductance and capacitance, and

$$Y_s = G_s + i\omega C_s \qquad (2)$$

$$Y_{el} = G_{el} + i\omega C_{el} \qquad (3)$$

where the subscripts s and el refer to the sample and electrode, respectively. The dielectric properties of the sample are obtained from Eq. (2) as:

$$\varepsilon_s' = \frac{C_s}{C_o} \qquad (4)$$

$$\varepsilon_s'' = \frac{G_s}{\omega C_o} \qquad (5)$$

where C_o is the vacuum capacitance of the sample. In practice, ε' and ε'' values are extracted from Y_{app} by a fitting procedure described as follows.

It is known that the frequency dependence of dielectric relaxations can be modeled by Havriliak–Negami function, which reduces to the Cole–Cole equation for symmetric distributions of relaxation times.[17,18] Because Havriliak–Negami fits to the data yielded curves indistinguishable from the results obtained from the Cole–Cole equation, the latter was adopted for the data of this article. A d.c. conductivity term, proportional to the reciprocal of frequency, was added to a sum of Cole–Cole expressions given as:

$$\varepsilon_s^* = -i\frac{\sigma_{dc}}{\varepsilon_o\omega} + \varepsilon_\infty + \sum_j \frac{(\Delta\varepsilon)_j}{\left[1 + (i\omega\tau_j)^{1-\delta j}\right]} \qquad (6)$$

where σ_{dc} is the d.c. conductivity, $(\Delta\varepsilon)_j$ is the strength of the jth dielectric relaxation, δ_j is the jth relaxation time distribution parameter, ε_o is the permittivity of free space (8.854 pF/m), τ_j is the characteristic relaxation time of the jth relaxation, and ε_∞ is the high frequency relative permittivity.

To analyze the data, the real and imaginary parts of Eq. (6) are substituted into Eq. (1) using the definition in Eqs. (4) and (5). A global fitting procedure consisting of a least squares non-linear fit to the frequency-dependent data was carried out using σ_{dc}, $(\Delta\varepsilon)_j$, τ_j, δ_j, ε_∞, and Y_{el} as fitting parameters. A fit to the data was considered successful if the calculated values were within 1% of the measurements, i.e. within the nominal experimental uncertainty of the observations. The fitting procedure began by considering initial values of σ_{dc} and Y_{el} in conjunction with one dielectric relaxation. If the 1% criterion for a good fit was not obtained, then additional relaxation dispersions were added to the fitting function one at a time until the 1% criterion was satisfied. For on-line measurements, the maximum number of relaxations used in the fitting function was two, i.e. j sums from 1 to 2.

RESULTS AND DISCUSSION

Morphology of the composites

Morphological characterization of the composites was carried out by TEM and XRD. Two TEM micrographs of nylon 6/30B nanocomposite indicating a high degree of exfoliation with traces of clay aggregates are shown in Fig. 2(A) and 2(B). A clay aggregate was found in Fig. 2(B) yet it is clear from Fig. 2(A) that most of the 30B silicate layers were well delaminated and were evenly distributed throughout the nylon 6 matrix. Two TEM micrographs of nylon 12/30B nanocomposite illustrating an intercalated state are shown in Fig. 3(A) and 3(B). The disappearance of the layered structures of 30B in the nylon 6 matrix can be supported by the XRD results seen in Fig. 4(A) where the characteristic silicate peak has shifted below $2\theta = 2°$, which is beyond the instrument sensitivity. The state of agglomeration/exfoliation in nylon 6/15A composite is confirmed by the XRD result shown in Fig. 4(A), where the characteristic clay peak indicated a d-spacing of around 3.34 nm. Nylon 6/30B composite is substantially more exfoliated than nylon 6/15A. 30B silicate, which bears hydroxyl functional groups, underwent a higher degree of exfoliation during melt compounding with nylon 6 resin compared to the non-polar 15A silicate.

It is seen from Fig. 4(A) and 4(B) that non-polar 15A silicate remained in an aggregate/exfoliated state in both of the
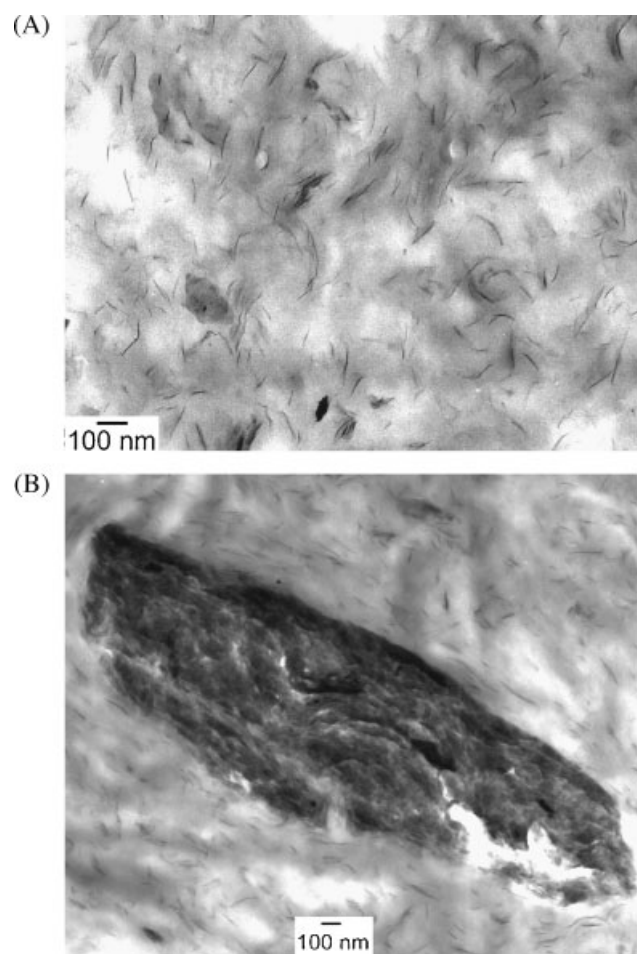
Figure 2. Two TEM micrographs with different resolutions of nylon 6/4% 30B nanocomposite showing a well-exfoliated microstructure with trace of aggregate.

(A)

(B)
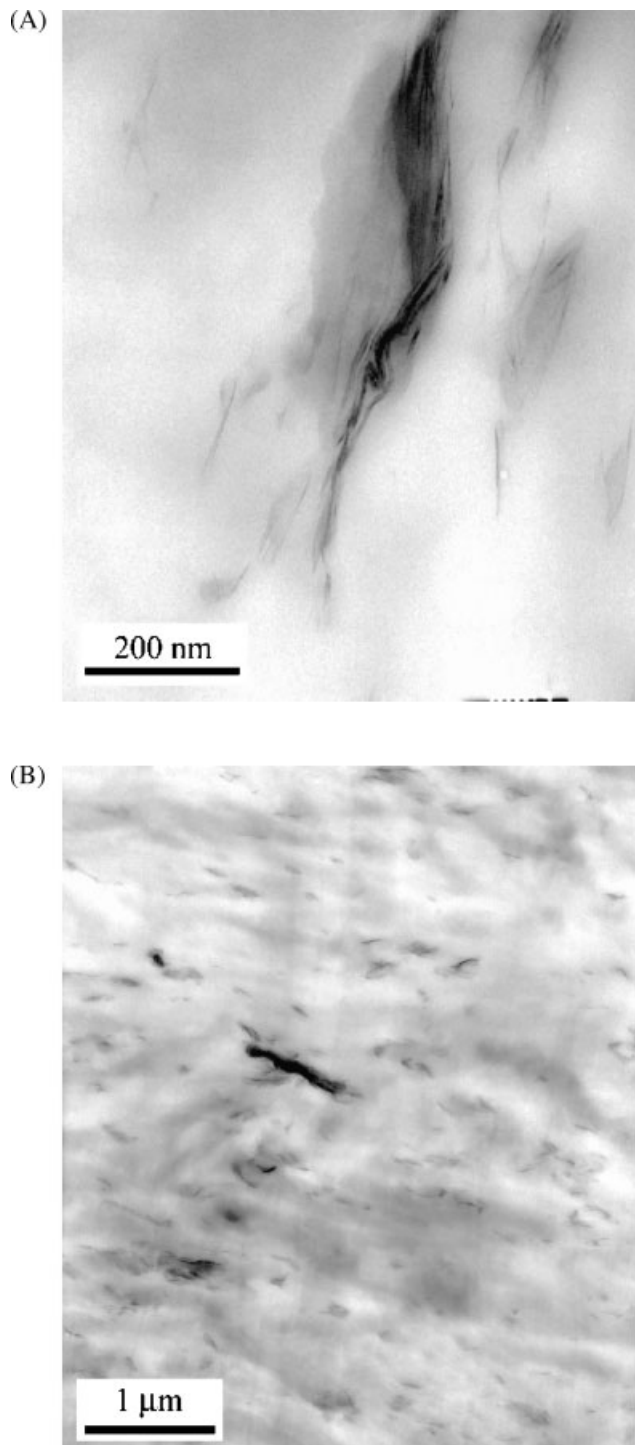
Figure 3. Two TEM micrographs with different resolutions of nylon 12/4% 30B nanocomposite showing an intercalated microstructure with traces of aggregates.

nylon matrices after extrusion even with extra ionic surfactants incorporated prior to mixing. It is therefore concluded that the dominant driving force to optimize the clay dispersion throughout the nylon matrix is the polymer/filler compatibility, which is enhanced by the functionality of the 30B surfactant possibly via hydrogen bonding. The amount of incorporated long chain organic surfactants serves to expand the clay galleries prior to compounding yet the complete delamination process is still governed by the thermodynamics.[19]

(A)

(B)
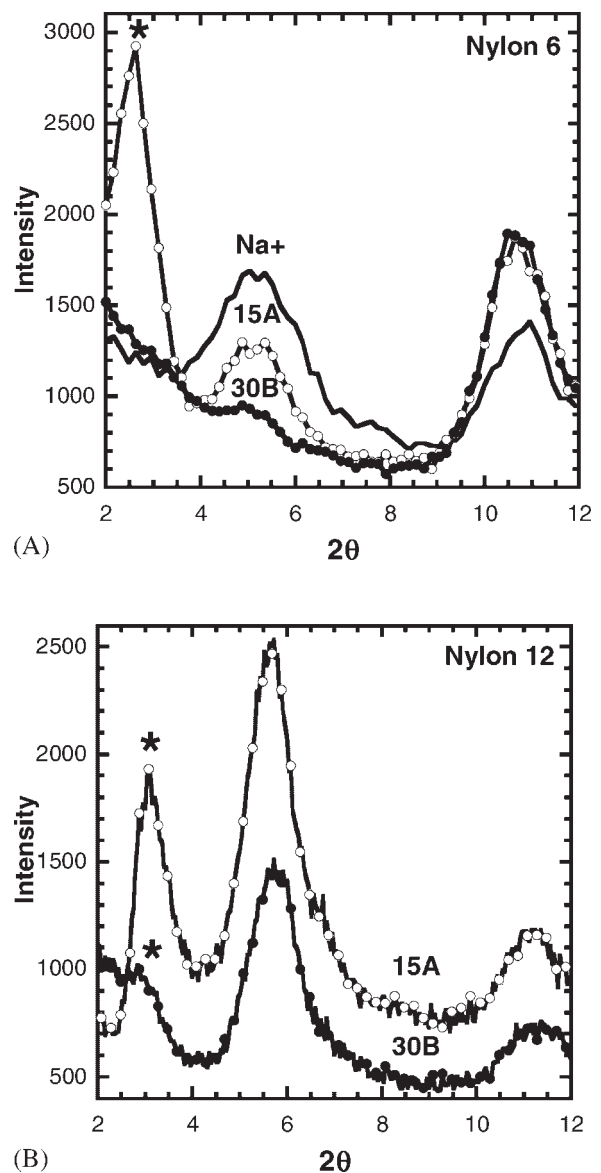
Figure 4. XRD results indicate: (A) an aggregate/exfoliated 15A and an exfoliated 30B with nylon 6 matrix and (B) an aggregate/exfoliated 15A and an intercalated 30B with nylon 12 resin. The asterisk identifies a peak in the curve with a *d*-spacing of 3.34, 2.87, and 3.11 nm for nylon 6/15A, nylon 12/15A, and 30B/nylon 12, respectively.

Figure 5(A) exhibits the measured on-line dielectric data for the nylon 12/30B composites taken at $T = 195°C$. An upswing in ε'' in the low frequency regime, resulting from ionic conduction above the glass transition temperature (T_g), is observed and the monotonic rise of ε' with descending frequency is due to the electrode polarization. The solid lines in both ε' and ε'' are the fits to the measured data using the Cole–Cole function corrected for ionic conduction and electrode polarization. The large discrepancy between the solid line and the dotted line shown in Fig. 5(A), best seen in the low frequency regime, is attributed to the electrode polarization caused by the pileup of ions at the electrode surface. This large deviation supports our hypothesis that the original Cole–Cole function has to be modified in order for material dielectric properties to be extracted. No relaxation is
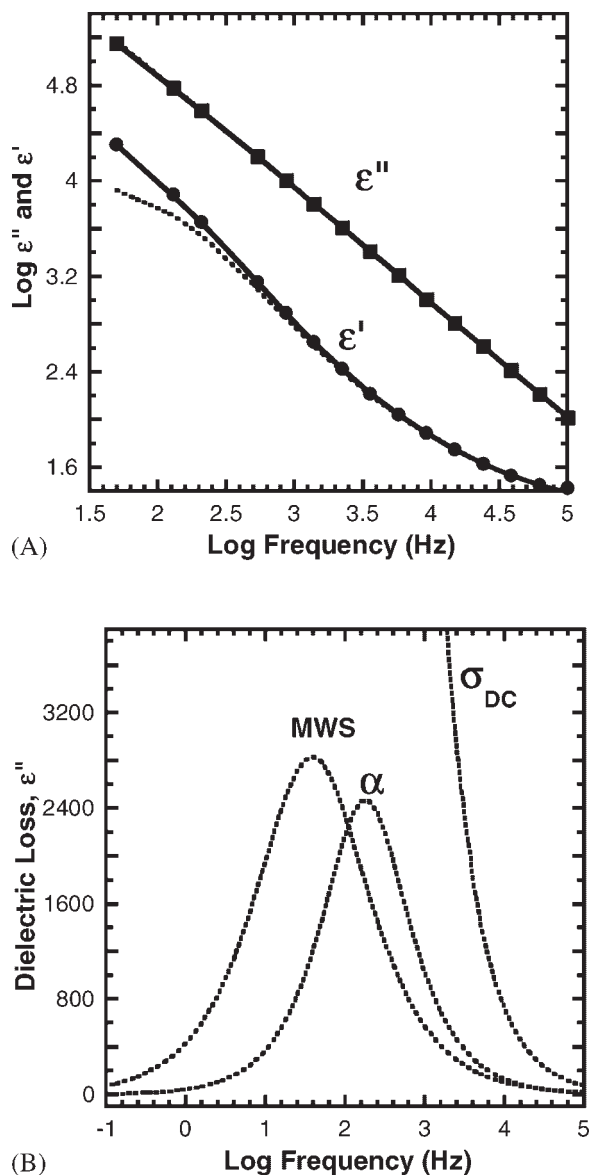
Figure 5. (A) Permittivity (ε') and dielectric loss (ε'') are plotted as a function of experimental frequency in the logarithmic scale for the nylon 12/30B at 195°C. Solid symbols are the measured data, dashed lines represent curves fitted by the original Cole−Cole equation, and the solid line illustrates results fitted by the Cole−Cole function corrected for d.c. conductivity and electrode polarization. (B) Two relaxation modes, Maxwell−Wagner−Sillars polarization (MWS) and α relaxation, along with d.c. conductivity extracted from the fitted ε'' were plotted as a function of frequency.

Table 1. Summary of online curve-fitting results including frequency (f), dielectric strength ($\Delta\varepsilon$), width of relaxation time distribution (δ), dielectric constant at infinite frequency (ε_∞), d.c. conductivity (σ_{dc}). The percentage of deviation between calculated and corrected ε' which indicates the degree of electrode polarization (EP, %) is also listed

	Nylon 6	Nylon 12
log f (Hz)	2.31 ± 0.04	2.06 ± 0.02
$\Delta\varepsilon$	548 ± 40	186 ± 2
δ	0.17 ± 0.01	0.1 ± 0.01
$\sigma_{dc} \times 10^4$ (S/m)	3.3 ± 0.1	0.34 ± 0.01
ε_∞	31.6 ± 0.1	20 ± 0.1
EP (%)	90 ± 1	64 ± 1

Table 2. Summary of on-line curve-fitting results

	Nylon 6/15A (2%) Aggregate/ exfoliated	Nylon 6/15A (4%) Aggregate/ exfoliated	Nylon 12/15A (4%) Aggregate/ exfoliated
log f (Hz)	2.84 ± 0.09	2.83 ± 0.03	2.69 ± 0.03
log f_{MWS} (Hz)	1.89 ± 0.04	1.90 ± 0.06	2.13 ± 0.02
$\Delta\varepsilon$	551 ± 200	956 ± 80	3451 ± 150
$\Delta\varepsilon_{MWS}$	$15\,057 \pm 2000$	$26\,166 \pm 500$	$13\,349 \pm 250$
δ	0.08 ± 0.04	0.04 ± 0.01	0.03 ± 0.01
δ_{MWS}	0.15 ± 0.01	0.14 ± 0.01	0.13 ± 0.01
$\sigma_{dc} \times 10^4$ (S/m)	9.3 ± 0.2	14.2 ± 0.1	5.7 ± 0.2
ε_∞	32.2 ± 0.6	44 ± 0.5	16.4 ± 0.8
EP (%)	65 ± 4	62 ± 0.1	55 ± 1

Table 3. Summary of on-line curve-fitting results

	Nylon 6/30B (2%) Exfoliated	Nylon 6/30B (4%) Partially exfoliated	Nylon 12/30B (4%) Intercalated
log f (Hz)	2.45 ± 0.05	2.47 ± 0.07	2.23 ± 0.03
log f_{MWS} (Hz)	0.65 ± 0.04	0.67 ± 0.07	1.59 ± 0.04
$\Delta\varepsilon$	1982 ± 300	3460 ± 900	5651 ± 450
$\Delta\varepsilon_{MWS}$	6464 ± 350	5387 ± 900	8308 ± 200
δ	0.14 ± 0.01	0.10 ± 0.01	0.083 ± 0.03
δ_{MWS}	0.04 ± 0.02	0.02 ± 0.01	0.2 ± 0.04
$\sigma_{dc} \times 10^4$ (S/m)	7.8 ± 0.1	12.3 ± 0.2	3.93 ± 0.1
ε_∞	27.3 ± 0.1	25.4 ± 0.3	16.7 ± 0.9
EP (%)	86 ± 2	87 ± 2	57 ± 1

visualized from either ε'' or ε' raw data, yet two relaxations along with a d.c. conductivity were retrieved from the fitting procedure as illustrated in Fig. 5(B). Two relaxation modes in the nylon 12/30B composite, centered at log frequency (f) = 1.6 and 2.2, are ascribed to MWS polarization[7–10] and α relaxation, respectively. The low frequency relaxation, MWS, arises from the conduction of surfactant ions that are dissociated from the silicate filler upon delamination. MWS shows a much broader relaxation time distribution ($\delta_{MWS} = 0.22$) than the higher frequency α relaxation

($\delta = 0.072$). The presence of filler/polymer interfaces broadens the MWS relaxation time distribution as each interface, bearing various interfacial geometries, is polarized at a distinct time scale. However, α relaxation in the polymer melt originates from the segmental dynamics of amorphous chains that exhibit relatively homogeneity for temperature well above the T_g value where T_g for nylon 12 is approximately 50°C.

All the fitting parameters are summarized in Tables 1−3. For all the composites, two relaxations were obtained from the fitting procedure, however, for the neat resins, only one relaxation was observed. The composites exhibited greater

d.c. conductivity than the neat polymers, owing to the presence of additional ions from the clays. MWS dispersion is identified by its large intensity, $\Delta\varepsilon_{MWS}$. Conducting ions accumulated at the resin/filler interface that move through the molten nylon under the influence of an applied voltage are responsible for the large $\Delta\varepsilon_{MWS}$. The magnitude of the MWS relaxation is much greater than that for the α relaxation in the neat nylon produced by orientation of the molecular dipoles.

Effect of polymer matrix

In order to understand the effect of chain length or polarity of polyamides on the dielectric behavior, the measured and fitted ε' of nylon 6 and nylon 12 were overlapped and displayed in Fig. 6(A). Nylon 6 exhibited higher permittivity than nylon 12. A much greater discrepancy between the measured ε' and the material ε' obtained by fit is noted in nylon 6 than in nylon 12, which results from a much stronger degree of electrode polarization in the former.[20–22] Deviation between the raw data and the fitted curve terminated at a much lower frequency ($\log f = 3$) in nylon 12 than in nylon 6 ($\log f = 4$) denoting that the onset of electrode polarization occurs at a lower frequency for nylon 6 resin.

The extracted relaxations along with the measured ε'' for both resins are displayed in Fig. 6(B). A slightly higher characteristic frequency in nylon 6 than in nylon 12 revealing faster α dynamics is shown. It is well documented[23–27] that the relaxation behavior of polyamides is governed by the concentration of intermolecular hydrogen bonding between amide groups, which is reversibly proportional to the number of aliphatic chains and is enhanced by the absorbed moisture. As such, more rapid segmental dynamics observed in nylon 6 is attributed to the greater moisture absorbed, which serves to plasticize the amorphous chains. The co-existence of plasticized and dry nylons relaxed at different time scales accounts for the slightly broader relaxation time distribution observed in nylon 6. All the fitting parameters for these two resins are summarized in Tables 1–3. The d.c. conductivity extracted from nylon 6 is one-order of magnitude higher than that from nylon 12. The ionic mobility in the plasticized polymer resin is enhanced yielding higher degree of d.c. conduction in nylon 6. The relaxation strength of the α relaxation, which is much greater in nylon 6, is a result of higher dipole concentration per unit volume for the shorter polyamide. In addition, the greater amount of water absorbed by nylon 6 can also form extra molecular dipoles with the polymer backbone, which would augment the dielectric magnitude.

Effect of filler and microstructures

To elucidate the impact of clay microstructures on the dielectric behavior of polyamides, the fitted ε'' for nylon 6 filled with 4% of 15A and 30B (partially exfoliated) were overlapped and displayed in Fig. 7(A) and 7(B). The dielectric loss of MWS and α relaxation for both composites are shown. It is noted that the incorporation of clay filler altered both relaxation modes yet in a distinct fashion.

The impact of the treated clay and the microstructures of the composites on the MWS interfacial polarization behavior
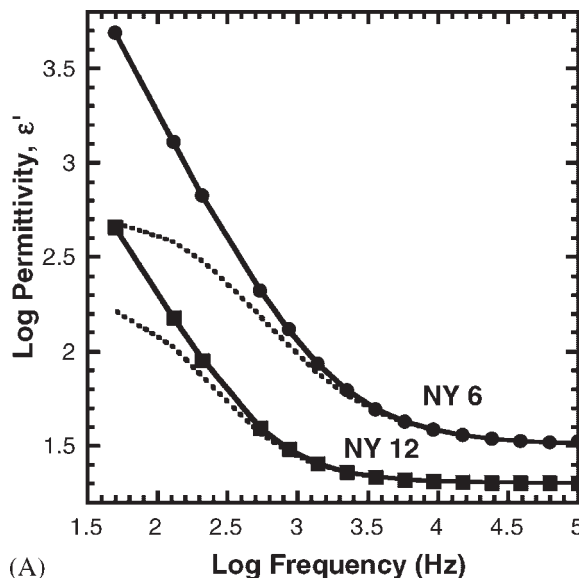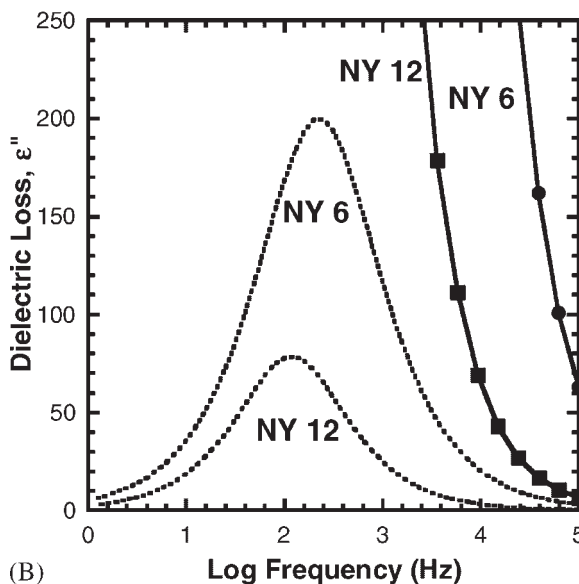
Figure 6. (A) Permittivity (ε') is plotted as a function of experimental frequency in the logarithmic scale for the neat nylon 6 (NY 6) and 12 (NY 12). Solid symbols are the measured data, dotted lines represent curves fitted by the original Cole−Cole equation, and the solid line illustrates results fitted by the Cole−Cole function corrected for d.c. conductivity and electrode polarization. (B) Dielectric loss (ε'') is plotted as a function of experimental frequency in the semi-logarithmic scale for the neat nylon 6 and 12. Solid symbols are the measured data, the dotted lines are the material dielectric dispersion (α relaxation) extracted from the fit and the solid lines are the fitted curves.

is demonstrated in Fig. 7(A). The disappearance of layered structure in the partially exfoliated 30B composite resulted in a progressively narrow MWS polarization ($\delta_{MWS} = 0.02$) compared to the aggregate/exfoliated 15A system ($\delta_{MWS} = 0.14$) as listed in Tables 2 and 3. It is the extra interfaces (polymer/filler and polymer/surfactant) created upon silicate delamination and small traces of aggregates (other than exfoliated nano-flakes) that are responsible for a
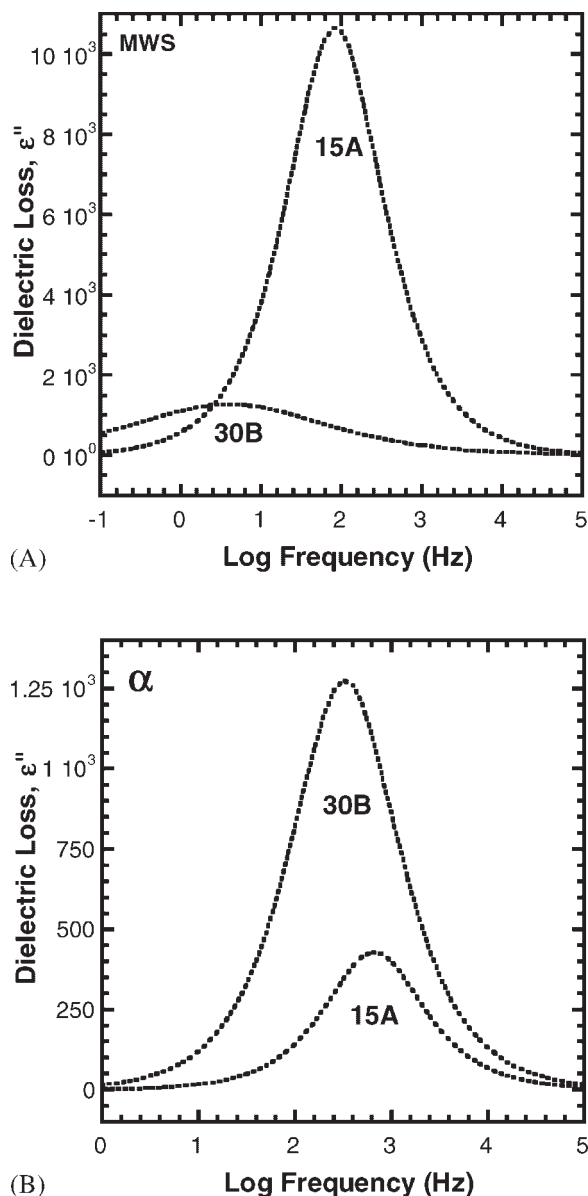
Figure 7. Dielectric loss (ε'') extracted from the corrected Cole–Cole fit is plotted as a function of experimental frequency in the semi-logarithmic scale for both of the nylon 6 filled with 4% mass fraction 15A and 30B. Two relaxation modes, Maxwell–Wagner–Sillars (MWS) polarization and α relaxation retrieved from curve fitting are plotted in (A) and (B), respectively.

wide distribution of characteristic frequencies. The MWS interfacial polarization is interpreted as an effective resistance–capacitance time constant ($\tau = RC$) of the resin/silicate medium where the resin behaves as the conducting resistance (R) and the silicate particle as the capacitance (C). In both composites, the conductivities (σ_{dc}) at processing temperature are approximately equal, which is 1.42×10^3 (S/m) for nylon 6/15A and 1.2×10^3 (S/m) for nylon 6/30B. Nevertheless, the capacitance of the 15A particle is much lower than the partially exfoliated 30B nanoparticles as the latter contains a large number of exfoliated platelets serving as nano-capacitors. Thus, the RC time constant of the 15A composite is shorter than that of the 30B composite leading to

a higher characteristic relaxation frequency ($\log f = 1.85$ Hz) for the aggregate/exfoliated 15A system. As seen in Tables 2 and 3, the MWS relaxation strength ($\Delta\varepsilon_{MWS}$) for the 4% of nylon 6/15A is fives times greater than that of 4% nylon 6/30B. This is a direct result of extra ionic surfactants incorporated by the manufacture in the 15A clay.

The impact of treated clay and microstructure of the composites on the α relaxation behavior is demonstrated in Fig. 7(B). The much higher α relaxation strength observed in the exfoliated 30B compared to the aggregate/exfoliated 15A is due to the delamination of silicate layers which enabled the ionic surfactants to be dissociated and to form extra molecular dipole moments via hydrogen bonding with the amide groups on the polymer backbone. All fitting parameters for nylon 6 and nylon 12 filled with 15A and 30B clay are summarized in Tables 2 and 3. All composites exhibited higher characteristic α relaxation frequencies than the neat resin with aggregate/exfoliated being the greatest. More rapid segmental motion upon the addition of silicate fillers is caused by dispersed fillers, which serve as "rigid molecular dividers" that diminish the degree of intermolecular cooperativity of the amorphous macromolecules. The size of cooperative domain, where segments relax simultaneously, was reduced as the whole polymer matrix was divided by numerous rigid silicate platelets. In addition to reducing intermolecular cooperativity, hindered motion of molecules adjacent to rigid filler surfaces also occurs. These two phenomena change relaxation dynamics in opposite directions because a diminished cooperativity increases the characteristic frequency and hindered motion reduces it. For the 15A aggregate composite, hindered motion is small compared to that seen for the 30B exfoliated silicate that exposes large surface area to the matrix polymer. For nylon/15A composite, interruption of intermolecular cooperativity is the dominant cause of the increase in molecular dynamics with respect to the neat polymer, whereas both reduced intermolecular cooperativity and hindered motion play significant roles for nylon/30B nanocomposite. In other words, effects due to inhibited chain mobility at nanoparticles surfaces were offset by diminished intermolecular cooperativity, resulting in a slightly slower chain dynamics found in the partially exfoliated 30B compared to the aggregate/exfoliated 15A. All 15A composites, regardless of resin types or clay loadings, yielded a slightly higher d.c. conductivity than 30B, which is a result of a greater surfactant concentration incorporated in the 15A silicate compared to that added in 30B.

Effect of filler concentration
To learn how the clay loading influences the dielectric behavior of polyamides, nylon 6 filled with 2 and 4% of 15A and 30B were prepared. All fitting parameters are listed in Tables 2 and 3.

For both 15A and 30B composites, only the dielectric intensity and d.c. conductivity were changed upon varying the filler concentration and all other relaxation features remain intact. Filling polymer resins with more silicate fillers would translate to a greater number of ionic and mobile surfactants present in the matrix, which would have three direct impacts on the dielectric properties of the polymer.

Firstly, the orientation of molecular dipoles is facilitated accounting for the increase in $\Delta\varepsilon$ for the α relaxation. Secondly, the creation of extra interfaces is responsible for a higher $\Delta\varepsilon_{MWS}$ detected in the composite with 4% mass faction filler. Thirdly, the ionic conduction process was promoted resulting in a rise in d.c. conductivity.

CONCLUSIONS

The on-line dielectric data obtained in this study reveal molecular dynamics in the melt for these two important commercial polymers, nylon 6 and nylon 12. For the α relaxation in the neat polymer, a higher characteristic frequency, broader relaxation time distribution, and greater dielectric intensity for nylon 6 compared to nylon 12 was observed inferring that the former resin absorbed higher amount of moisture and the amorphous chains are more plasticized. Higher d.c. conductivity retrieved from the neat nylon 6 also advocated the fact that stronger protonic conduction was triggered in the presence of water.

Three prominent features, which differentiated the filled systems from the neat polymers, are disclosed from this study. Firstly, only one relaxation, α, was detected in the neat resin and yet two relaxations, α and MWS polarization, were retrieved from the composites regardless of the clay microstructures or filler loadings. The additional relaxation mode, MWS, is due to the polarization at the polymer/filler interfaces. The MWS dielectric relaxation, whose origin is conducting ions, was identified by its large intensity ($\Delta\varepsilon$) that is an order of magnitude greater than the intensity of the α relaxation associated with orientation of molecular dipoles. Secondly, the higher characteristic frequency for the α relaxation in the composites is due to a combination of diminished intermolecular cooperativity and hindered amorphous chain motion. The former effect dominates over the latter effect in the aggregate/exfoliated composites compared to the exfoliated one accounting for highest α frequency observed in the state of agglomeration/exfoliation. Thirdly, higher d.c. conductivity extracted from the composites compared to the neat resins is a direct result of incorporated ionic surfactants in the fillers.

Three markers, which distinguished the exfoliation from the agglomeration microstructures, were discovered from the on-line dielectric investigation. Firstly, the exfoliated nanocomposite exhibited a slower MWS relaxation than the aggregate composite suggesting a longer *RC* time constant that derives from the high capacitance of nano-sized exfoliated silicate particles. Secondly, the dynamics of the α relaxation change

significantly with the exfoliated microstructure displaying the lower characteristic frequency and the higher relaxation strength than the aggregate sample. The delaminated silicate layers inhibited the amorphous chain motion accounting for a decreased relaxation frequency and the dissociated ionic surfactants formed pseudo molecular dipole moments via hydrogen bonding, which resulted in a rise in the dielectric intensity. Thirdly, a higher degree of electrode polarization was manifested in the exfoliated system as the delamination of the silicates enabled the ionic surfactants to be dissociated and to migrate to the surface of electrodes.

REFERENCES

1. Alexandre M, Dubois P. *Mater. Sci. & Eng. R—Reports* 2000; **28**: 1–63.
2. Giannelis EP. *Adv. Mater*. 1996; **8**: 29–35.
3. LeBaron PC, Wang Z, Pinnavaia TJ. *Appl. Clay Sci*. 1999; **15**: 11–29.
4. Manias E, Touny A, Wu L, Strawhecker K, Lu B, Chung TC. *Chem. Mater*. 2001; **13**: 3516–3523.
5. Lu HB, Nutt S. *Macromolecules* 2003; **36**: 4010–4016.
6. Ren JX, Krishnamoorti R. *Macromolecules* 2003; **36**: 4443–4451.
7. Hedvig P. *Dielectric Spectroscopy of Polymers*. John Wiley & Sons: New York, 1977; 282–290.
8. Maxwell JC. *Electricity and Magnetism*. Oxford: Clarendon, 1892.
9. Sillars RW. *J. Inst. Elec. Eng*. 1937; **80**: 378.
10. Wagner KW. *Arch. Elektrotech*. 1914; **2**: 371.
11. Bur AJ, Roth SC, Lee YH, Noda N, McBrearty M. *Plast. Rubber Comp*. 2004; **33**: 5–10.
12. Bur AJ, Roth SC, Lee YH, McBrearty M. *Rev. Sci. Instrum*. 2004; **75**: 1103–1109.
13. Bur AJ, Roth SC, McBrearty M. *Rev. Sci. Instrum*. 2002; **73**: 2097–2102.
14. Perusich S, McBrearty M. *Polym. Eng. Sci*. 2000; **40**: 214–226.
15. Zaretsky MC, Li P, Melcher JR. *IEEE Trans. Electrical Insulation* 1989; **24**: 1159–1166.
16. Pizzitutti F, Bruni F. *Rev. Sci. Instrum*. 2001; **72**: 2502–2504.
17. Havriliak S, Negami S. *J. Polym. Sci., C—Polym. Symp*. 1966; **14**: 99.
18. Cole RH. *J. Chem. Phys*. 1955; **23**: 493.
19. Vaia RA, Giannelis EP. *Macromolecules* 1997; **30**: 7990–7999.
20. Pathmanathan K, Cavaille JY, Johari GP. *J. Polym. Sci., B—Polym. Phys*. 1992; **30**: 341–348.
21. Pathmanathan K, Johari GP. *J. Polym. Sci., B—Polym. Phys*. 1993; **31**: 265–271.
22. Pathmanathan K, Johari GP. *J. Chem. Soc.—Faraday Trans*. 1995; **91**: 337–341.
23. Boutros S, Rizk HA, Hanna A, Gerges MK. *J. Chim. Phys. Phys.-Chim. Biol*. 1979; **76**: 501–506.
24. Hanna AA. *Thermochim. Acta* 1984; **76**: 97–103.
25. Ikeda S, Matsuda K. *Jpn J. Appl. Phys*. 1980; **19**: 855–859.
26. Laredo E, Hernandez MC. *J. Polym. Sci., B—Polym. Phys*. 1997; **35**: 2879–2888.
27. Rele VB, Papir YS. *J. Macromol Sci.—Phys*. 1977; **B13**: 405–417.